Supplementary Information

Bifunctional PtAg-enabled oscillation electrorefining of PET waste-derived ethylene glycol and water for rapid glycolic acid and H_2 coproduction

Xin Hu,[a] Luliang Liao,[b] Li-Ming Yang,[a] Bao Yu Xia,*[a] and Bo You*[a]

[a]Key Laboratory of Material Chemistry for Energy Conversion and Storage, Ministry of Education, Hubei Key Laboratory of Material Chemistry and Service Failure, School of Chemistry and Chemical Engineering, Huazhong University of Science and Technology, Wuhan, Hubei 430074.

[b]School of Materials and Energy, Jiangxi Science and Technology Normal University, 589Xuefu Road, Nanchang, Jiangxi, 330031.

Correspondence and requests for materials should be addressed to: byxia@hust.edu.cn; youbo@hust.edu.cn

1. Chemicals and Materials

Tetraammineplatinum chloride hydrate ($(NH_3)_4PtCl_4$, 55%Pt), silver trifluoroacetate ($C_2F_3O_2Ag$, 98%), glycollic acid ($C_2H_4O_3$, 98%) and tungsten carbonyl ($W(CO)_6$, 97%) were purchased from Aladdin. Acetic acid (CH_3COOH, 99.5%), ethanol (EtOH, 99.9%), hydrochloric acid (HCl, 37.0%), ethylene glycol ($(CH_2OH)_2$, 99.0%), potassium hydroxide (KOH, 85%), N, N-dimethylformamide (DMF, 99.8%) were purchased from Sinopharm Group. Deuterated water (D_2O) was purchased from Adamas Reagent. Ni foam (1.6 mm) was purchased form GUANG SHENG JIA NEW MATERIALS CO., LTD. Ultrapure water (18.2 MΩ cm) was used in all experiments.

2. Electrocatalysts Synthesis

A hydrothermal approach was used to synthesize the aimed electrocatalysts. A piece of nickel foam (NF) was cleaned by dilute hydrochloric acid solution, ethyl alcohol, and deionized water sequentially. After drying at room temperature for 12 h, the NF (1cm × 2cm × 1.6 mm) was transferred to a 25 mL Teflon-lined stainless-steel autoclave containing $(NH_3)_4PtCl_4$ (20 mg) or $C_2F_3O_2Ag$ (10 mg), $W(CO)_6$ (60mg), acetic acid (4 mL) and DMF (16 mL). The above mixture was sonicated for 30 min to get a transparent solution and then heated to 140 ^oC and kept for 24 h in an oven. Finally, the resulting samples were dried in an oven at 60 ^oC to obtain Pt/NF and Ag/NF controls. PtAg/NF-X were prepared with similar method by control the ratio of $(NH_3)_4PtCl_4$ and $C_2F_3O_2Ag$, PtAg/NF-1: 16mg $(NH_3)_4PtCl_4$ and 2 mg $C_2F_3O_2Ag$; PtAg/NF-2: 10mg $(NH_3)_4PtCl_4$ and 5 mg $C_2F_3O_2Ag$; PtAg/NF-3: 4mg $(NH_3)_4PtCl_4$ and 8 mg $C_2F_3O_2Ag$. PtAg/NF-2 represent PtAg/NF in the text. The similar and scale-up method was used to prepare the PtAg/NF electrocatalysts used in the continuous flow reactor: the NF (3 cm × 4 cm × 1.6 mm) was transferred to a 150 mL Teflon-lined stainless-steel autoclave containing $(NH_3)_4PtCl_4$ (60 mg), $C_2F_3O_2Ag$ (30 mg), $W(CO)_6$ (360 mg), acetic acid (24 mL) and DMF (96 mL). The above mixture was sonicated for 30 min to get a transparent solution and then heated to 140 ^oC and kept for 24 h in an oven. Finally, the resulting samples were dried in an oven at 60 ^oC to obtain PtAg/NF electrode.

3. Physiochemical Characterizations

The X-ray Diffraction (XRD) patterns were recorded using a Bruker D8 Advance X-ray diffractometer with Cu Kα irradiation (λ =1.5406 Å) operation at 40 kV and 40 mA. The scanning electrode microscopy (SEM) was performed using a TESCAN MIRA LMS microscope. The transmission electrode microscopy (TEM), high-resolution TEM and selected area electron diffraction pattern (SAED) were conducted on a JEOL JEM 2100F. X-ray photoelectron spectroscopy (XPS) was collected on scanning X-ray microprobe (PHI 5000 Verasa, ULAC-PHI, Inc.) using Al Kα radiation and the C1s peak at 284.8 eV as internal standard. Photoluminescence (PL) spectra were obtained at ambient temperature using a HitachiF-7000 fluorescence spectrophotometer with an excitation wavelength of 300 nm. EPR spectra of samples were collected on a JEOL JES-FA 200 EPR spectrometer with 5,5-Dimethyl-1-pyrroline N-oxide (DMPO) as the spin-trapping agent. The gas and liquid products during HER and EGOR were quantified by gas chromatography (GC, Panna A91 Plus) and ^{1}H NMR (Bruker AV400).

4. Electrocatalytic Measurements.

The electrochemical tests were conducted with CHI 760E electrochemical workstation (CH Instruments, Inc., Shanghai) in a typical three-electrode flow cell system at room temperature. For EG oxidation reaction (EGOR), 1 M KOH with 1 M EG solution was used as the electrolyte with a flow rate of 20 mL min^{-1}. All potentials stated were calibrated with respect to the reversible hydrogen electrode (RHE) obtained through RHE calibration using $E_{RHE} = E_{Ag/AgCl} + 0.198 + 0.059\times pH$, where the pH value was tested by a pH meter (FE28, Mettler Toledo, Switzerland). iR (current times internal resistance) compensation was applied in all electrochemical experiments. The as-prepared electrocatalysts-loaded electrodes and Ag/AgCl electrode were used as the working and reference electrodes, respectively. The pulse sequence was set as 0.8 V for 0.5 h and -0.8 V for 0.5 h as a cycle period.

The gas and liquid products were quantified by Panna A91 Plus GC and ^{1}H NMR, respectively. The produced H_2 is directly passed into by GC (Panna A91 plus) equipped with a molecular sieve PQ packed column (1/8 inch, 1m), a 5A packed column (1/8 inch,

3m), and a thermal conductivity detector. The oven temperature was maintained at 60 ^{o}C and argon is used as the carrier gas and standard gas with different H_2 concentrations are sequentially introduced into by GC for quantification toward construction of calibration curves. Because the amount of the generated H_2 in continuous flow reactor with larger PtAg/NF electrode is too large, exceeding the range of GC (which is suitable for trace analysis), so the gas produced in flow cell was quantified with a gas burette. The Faradaic efficiency (FE) for H_2 generation was calculated by the following equation:

$$FE_{H2} = zFPV/RTQ \times 100\%$$

wherein z is the transfer number of electrons for H_2 gas (2), V is the volume concentration of gas product, Q is the pass charge during electrolysis which can be obtained via the electrochemical workstation. P is the atmospheric pressure (1.01×10^5 Pa), T is the room temperature, F is the Faraday constant (96485 C mol^{-1}) and R is the idea gas constant (8.314 J mol^{-1} K^{-1}).

NMR samples were prepared by mixing 200 uL D_2O, 100 uL DMSO (6 mM) and 300 uL obtained solution. The calibration curves were constructed by replacing obtained solution with standard formate, GA and EG solutions at specific concentrations with DMSO as the internal standard substance. The Faradaic efficiency (FE) for GA and formate generation was calculated by the following equation:

$$FE_{GA} = \text{generated GA } (mol) \times 4 \times 96485/Q \text{ (the amount of charge)} \times 100\%$$

$$FE_{formate} = \text{generated formate } (mol) \times 3 \times 96485/Q \text{ (the amount of charge)} \times 100\%$$

5. Quasi-In-Situ EPR Characterizations

The radicals were electrochemically generated by performing a constant potential electrolysis in a specified solution, and trapped by the 5,5-dimethyl-l-pyrroline-N-oxide (DMPO) for the analysis of EPR (JES FA200 EPR spectrometer). For the EPR measurement of ·DMPO-OH radicals, PtAg/NF and Pt/NF electrodes were applied as the working electrodes in 1 M KOH electrolyte. Followed by Ar gas bubbling to remove

oxygen, the electrolyte was electrolyzed at the potential of 0.80 V vs RHE for 1 min, 100 μL of the reaction solution was collected from the electrolyte, and mixed with 100 μL of 0.1 M DMPO solution to trap the generated ·OH. For the EPR measurement of the ·DMPO-CH_2OH radical, the electrolyte changes from 1 M KOH to 1 M KOH containing 1 M EG, and similar measurements were conducted.

6. Operando ATR-FTIR Spectroscopy Measurements

Chemical Deposition of Au Film on Single Crystal Si: A thin Au film was chemically deposited on single Si crystals according to a previous report.[1-3] Specifically, 0.105 g NaOH was dissolved in 67 mL deionized water and mixed with 3 mL $HAuCl_4$ (0.1 g mL^{-1}) to obtain an orange-red solution A. Thereafter, 0.1337 g NH_4Cl, 0.6025 g $Na_2S_2O_3·5H_2O$, and 0.9653 g Na_2SO_3 were dissolved in 30 mL deionized water to obtain solution B. Then 7 mL solution A and 3 mL solution B were mixed and stirred for at least 3 h until the mixture became clear. The resulting solution was denoted as solution C. Before chemical deposition of Au, the Si crystal was polished with 50 nm Al_2O_3 powder for 10 min and then soaked in piranha solution (6 mL 98% H_2SO_4 and 2 mL 30% H_2O_2) for 1 h, and finally washed with deionized water and ethanol, making the surface of Si crystal hydrophobic. Next, the Si was immersed in 40% NH_4F for 90 s, and immediately immersed in a mixture of 4 mL solution C and 34 uL 40% HF at 55 °C for 5 min to form a thin Au film after washing with deionized water and ethanol.

Loading of Electrocatalysts over Au Film-Coated Si Crystal: The electrocatalyst ink was prepared by dispersing 20 mg catalyst powder in a solution containing 2.9 mL isopropanol and 100 μL 5 wt % Nafion solution followed by ultrasonication for 1 h. Then, 50 μL of the catalyst ink was dropped onto the Au film coated Si crystal and left to dry slowly.

Operando ATR-FTIR measurements: the ATR-FTIR was performed on a Thermo-Fisher Nicolet™ iS20 FTIR spectrometer equipped with a liquid nitrogen-cooled HgCdTe (MCT) detector using a VeeMax III ATR accessory (Pike Technologies). A germanium prism (60°, PIKE Technologies) was mounted in a PIKE electrochemical three-electrode cell with an Ag/AgCl reference electrode (Pine Research) and a

platinum-wire counter electrode. All ATR-FTIR measurements were acquired by averaging 64 scans at a spectral resolution of 4 cm^{-1}. 1 M KOH with 1 M EG after purging Ar with 30 min was used as the electrolyte was for EGOR. A CHI 760E electrochemical workstation (CH Instruments, USA) was connected for chronoamperometric tests from 0.1 to 1.0 V vs RHE for EGOR.

7. Theoretical Calculations

Computational Methods: All calculations were performed using the periodic spin-polarized DFT calculations with the projector augmented wave (PAW) method implemented in the Vienna Ab Initio Simulation Package (VASP),[4-6] the kinetic energy cutoff of 400 eV was used for a plane wave basis set. The exchange correlation energy was used with the generalized gradient approximation (GGA) and Perdew-Burke-Ernzerhof (PBE).[7] A 5×5×1 *k*-point grid was used for sampling the Brillouin zone.[8] The electronic convergence was set to 5×10^{-6} eV and the forces converge to 0.03 eV $Å^{-1}$.

For the adsorption process of of the species involving in Pt and PtAg catalysts were defined by Eqs. (1):

$$E_{ads} = E_{species} + E_{slab} - E_{slab/species} \quad (1)$$

Where $E_{species}$ and E_{slab} were the total energy of the adsorbate and bare surface directly obtained from DFT calculations, respectively, and $E_{slab/species}$ was the total energy of optimized adsorbate-surface.

For an elementary reaction, reaction energy (ΔH) were calculated by Eqs. (2):

$$\Delta H = E_{FS} - E_{IS} \quad (2)$$

Where E_{IS} and E_{FS} were the total energies of reactant and final state directly from DFT calculation, respectively.

To understand the underlying electronic properties, the electronic structure in term of *d*-band center of Pt and PtAg catalysts were investigated, *d*-band center (eV) values were obtained by Eqs. (3):

$$\varepsilon_d = \frac{\int_{-\infty}^{Ef} E\rho_d(\mathrm{E})\,\mathrm{dE}}{\int_{-\infty}^{Ef} \rho_d(\mathrm{E})\,\mathrm{dE}} \quad (3)$$

Where ρ_d represented the density of states projected onto Pt and PtAg atom's *d*-band and E_f was the Fermi energy.

Computational Models: For the Pt/NF catalyst, the Pt(111) surface is the most stable facet, which also has the most dominantly exposed crystal facets with the lowest surface energy, so it was generally chosen as the representative surface for experimental and theoretical studies. Thus, in this study, the flat Pt(111) surface was employed to investigate the oxidation step of EG, a three-layer *p*(4×4) Pt(111) was cleaved from the the optimized lattice parameter of 3.9123 Å, in line with the experimental lattice parameter of 3.9239 Å. The vacuum gap was set to 15 Å to separate the slabs, which was large enough to avoid interactions between the slabs. During the calculations, the bottom one layers was fixed at their bulk positions, whereas the top two layers and all adsorbed species were relaxed.

To probe the synergistic effect between Pt and Ag atoms in PtAg/NF, one Pt atom of unit cell were replaced by Ag atom to construct PtAg bimetallic unit cell, a three-layer *p*(2 × 2) PtAg(111) was cleaved to model the bimetallic PtAg, which was separated by a vacuum distance of 15 Å. During the calculations, the bottom one layers was fixed at their bulk positions, whereas the top two layers and all adsorbed species were relaxed.

8. Supplementary Figures and Tables

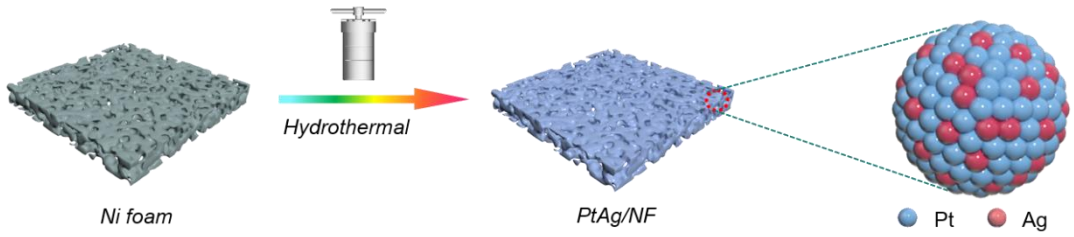

Fig. S1 Schematic for the preparation of bifunctional PtAg/NF electrocatalyst.

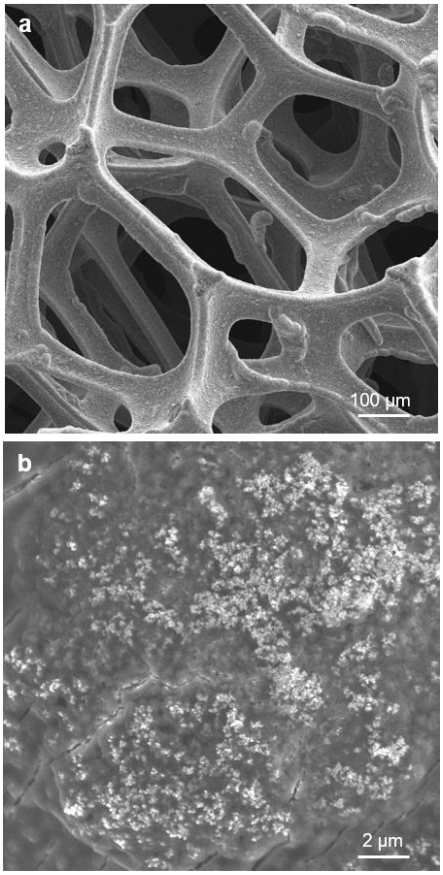

Fig. S2 SEM images of PtAg/NF at different magnifications.

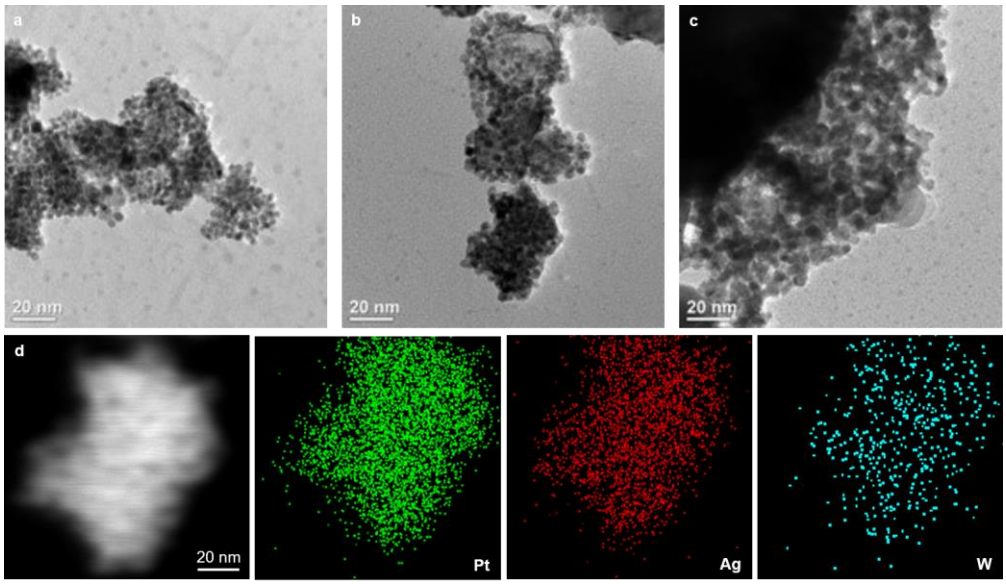

Fig. S3 High-magnification TEM images of a) Pt/NF, b) PtAg/NF and c) Ag/NF. (d) Element mapping images of PtAg/NF.

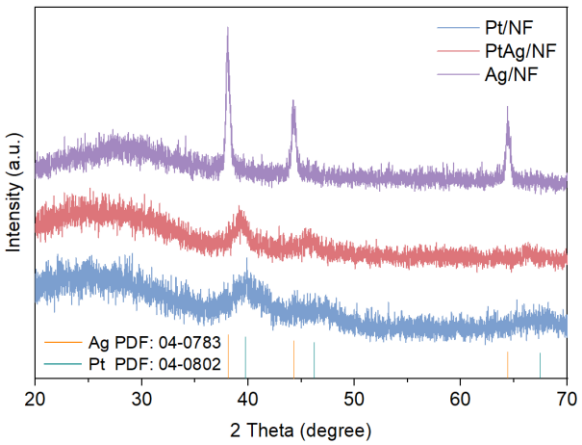

Fig. S4 XRD patterns of Pt, Ag and PtAg active species for the relevant Pt/NF, Ag/NF and PtAg/NF sample. *Note that to avoid the interferance of Ni foam, the active speces were detached from the resulting electrocatalysts via ultrasonication.*

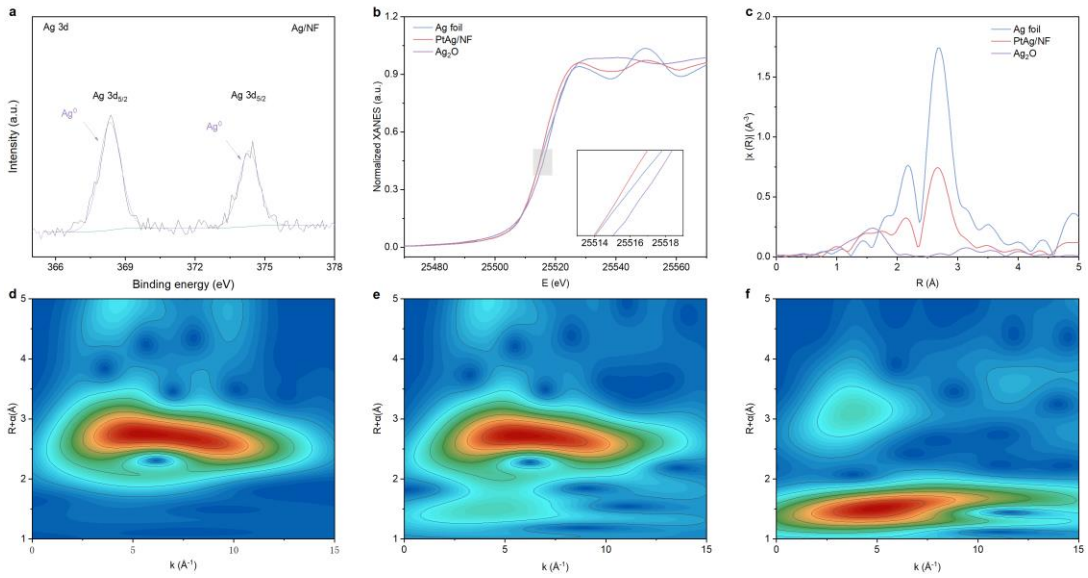

Fig. S5 a) High-resolution Ag 3d XPS spectrum of Ag/NF. b) Normalized Ag K-edge XANES spectra of Ag foil, PtAg/NF, Ag_2O. c) FT $k^2\chi(R)$ Ag K-edge EXAFS spectra for Ag foil, PtAg/NF and Ag_2O. d-f) WT for the Ag K-edge EXAFS signals of Ag foil, PtAg/NF and Ag_2O.

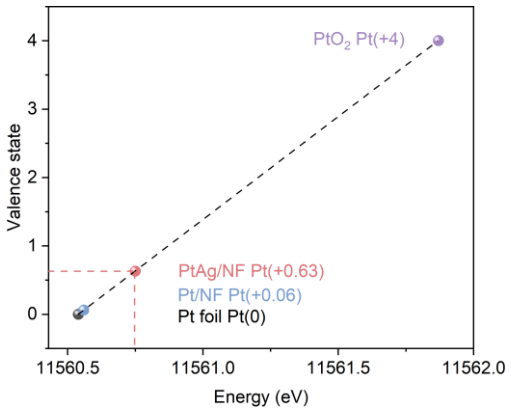

Fig. S6 Average valence state fitting of Pt from the XANES spectra.

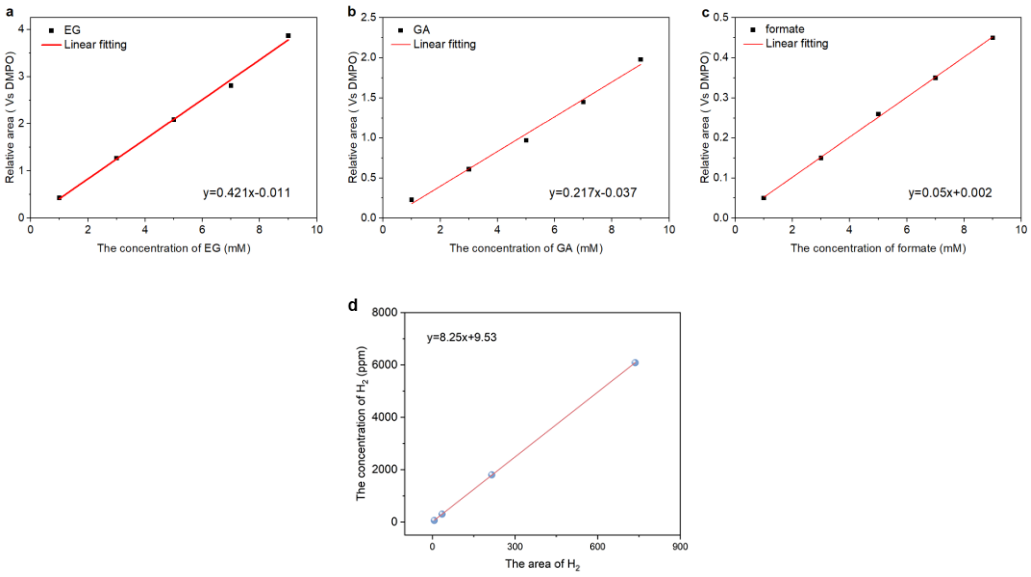

Fig. S7 Calibration curves of a) EG, b) GA, c) formate and d) H_2.

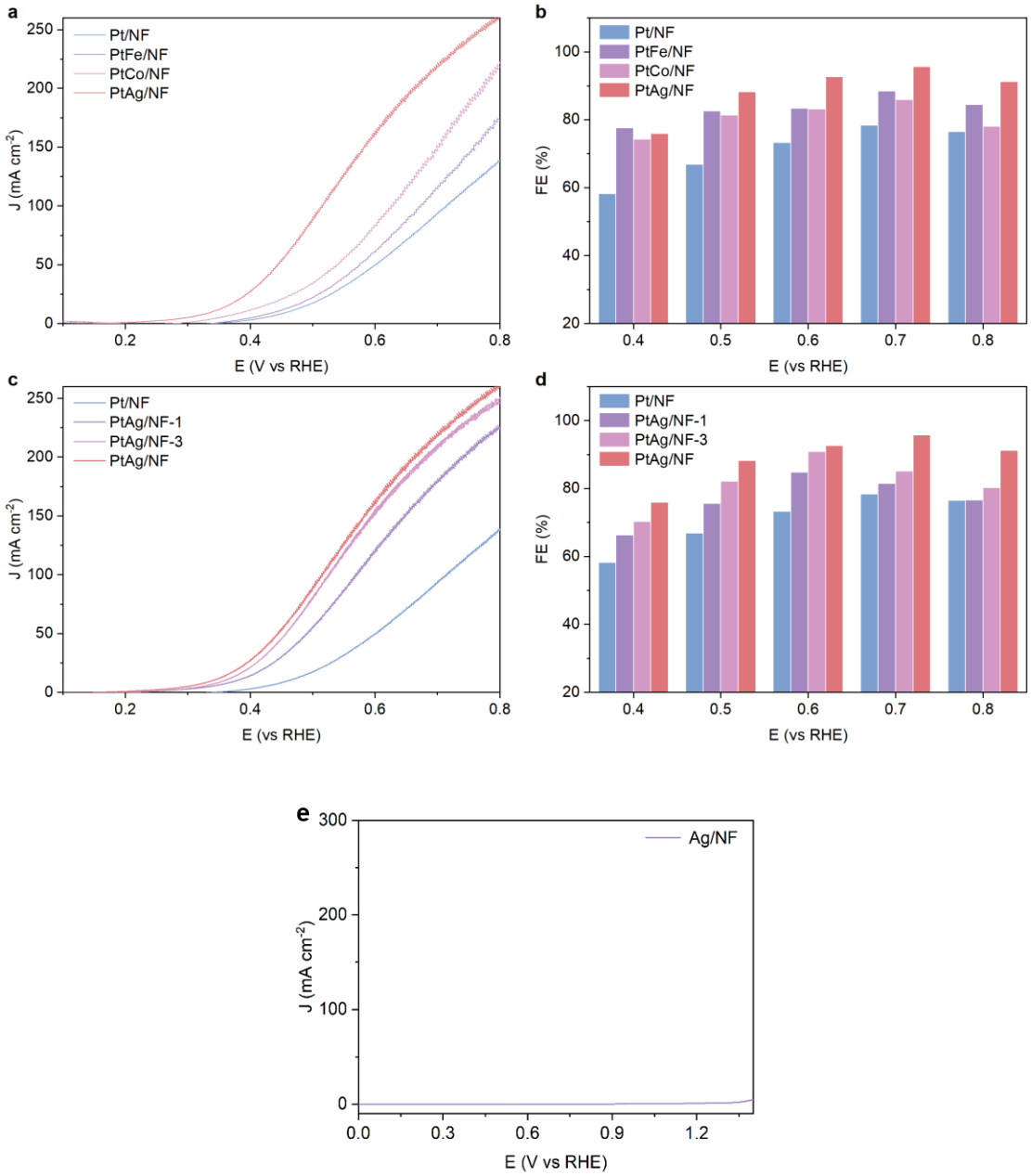

Fig. S8 a) LSV curves and b) FE_{GA} of Pt/NF, PtFe/NF, PtCo/NF and PtAg/NF in 1 M KOH with 1 M EG, c) LSV curves and d) FE_{GA} of Pt/NF, PtAg/NF-1, PtAg/NF-3 and PtAg/NF in 1 M KOH with 1 M EG. e) LSV curves of Ag/NF in 1 M KOH with 1 M EG. *Note that the Ag/NF shows negligible EGOR activity under investigated potential window*.

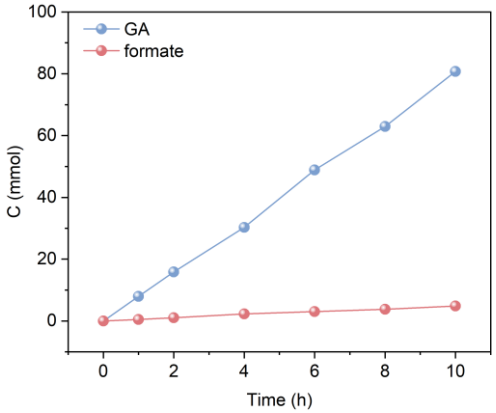

Fig. S9 Intermediates analysis and the time curves of PtAg/NF.

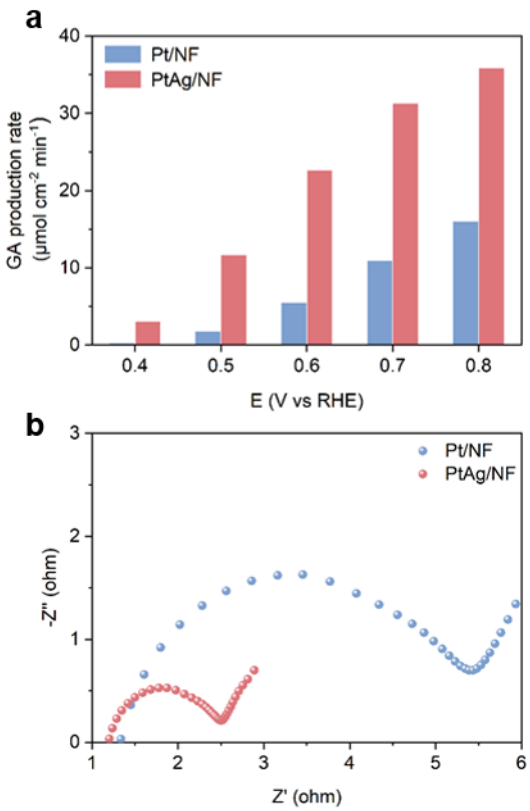

Fig. S10 a) GA production rate of Pt/NF and PtAg/NF at various potentials, and b) electrochemical impedance spectra of Pt/NF and PtAg/NF in 1 M KOH with 1 M EG measured at 0.6 V vs RHE.

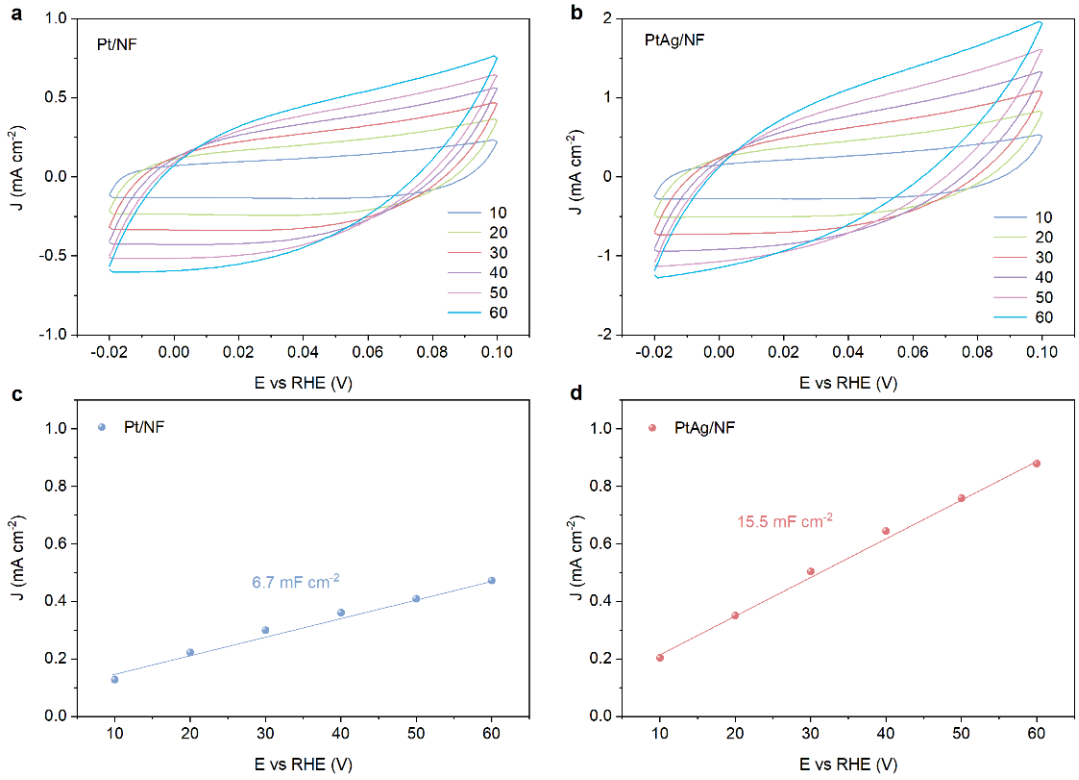

Fig. S11 Cyclic voltammograms of a) Pt/NF and b) PtAg/NF in the non-Faradaic region with scan rates from 10 to 60 mV s^{-1}. Scan rates dependence of the current densities of c) Pt/NF and d) PtAg/NF.

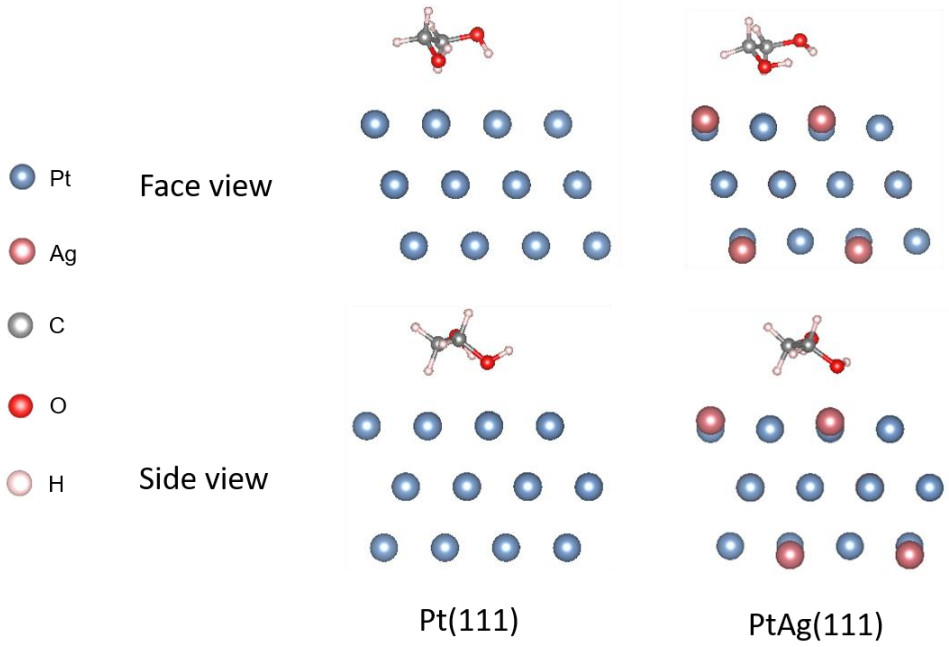

Fig. S12 Optimized *EG on Pt(111) (left) and PtAg(111) (right).

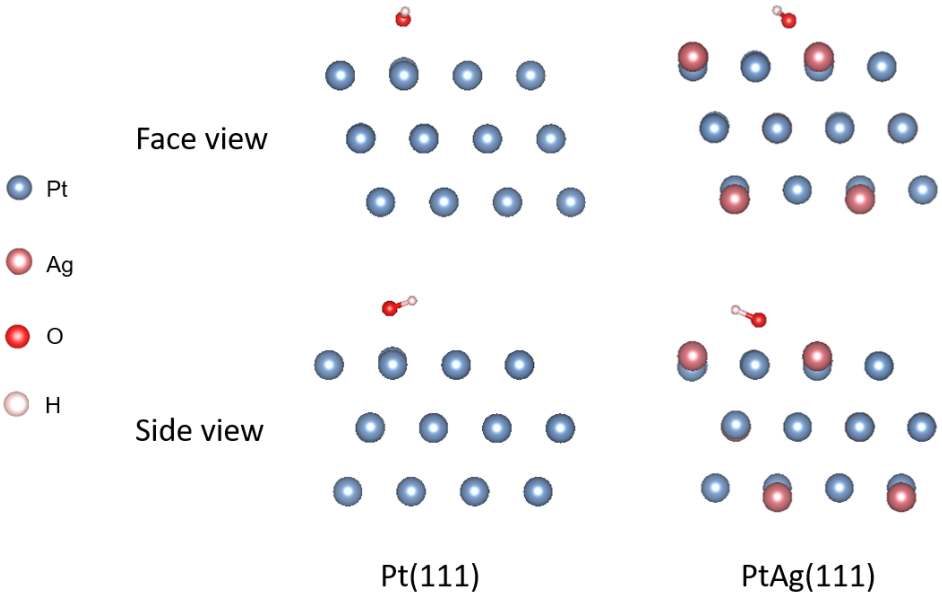

Fig. S13 Optimized *OH on Pt(111) (left) and PtAg(111) (right).

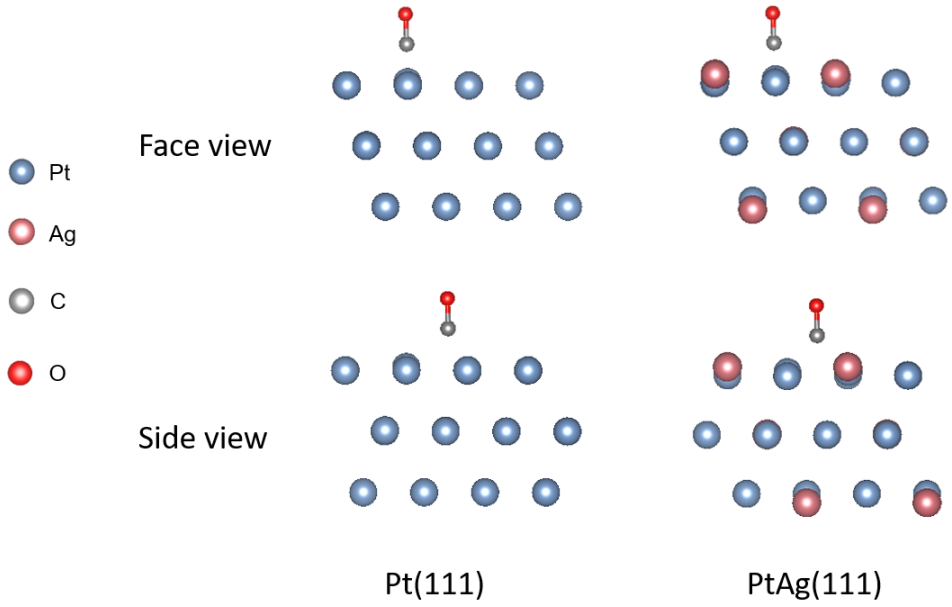

Fig. S14 Optimized *CO on Pt(111) (left) and PtAg(111) (right).

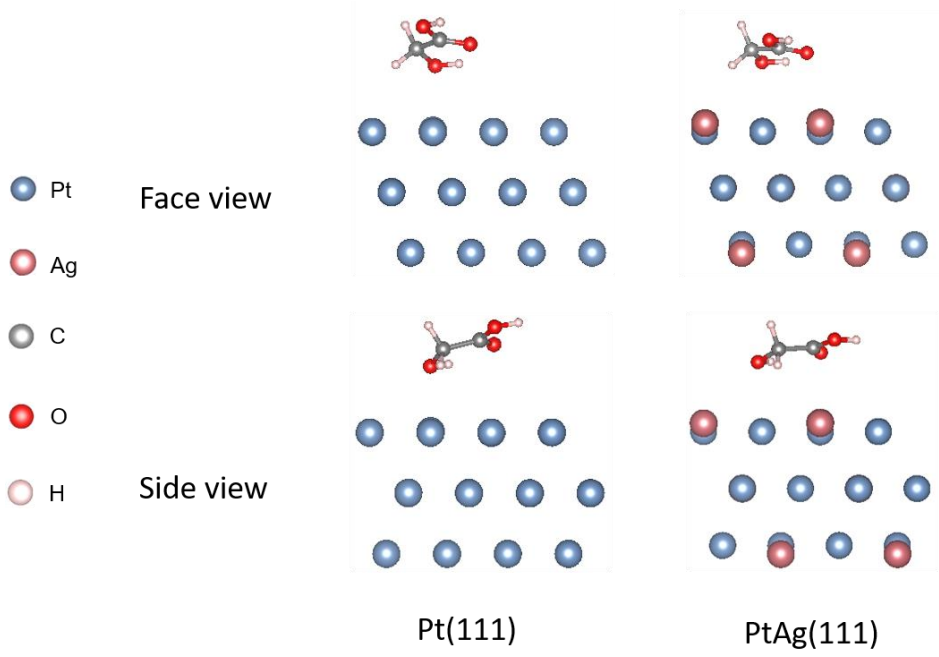

Fig. S15 Optimized *GA on Pt(111) (left) and PtAg(111) (right).

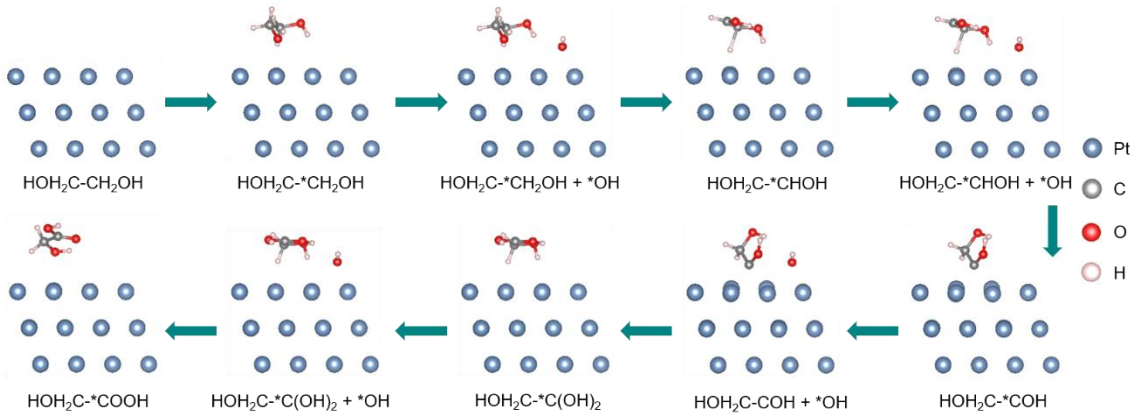

Fig. S16 The optimized configurations of the EG oxidation process on Pt(111).

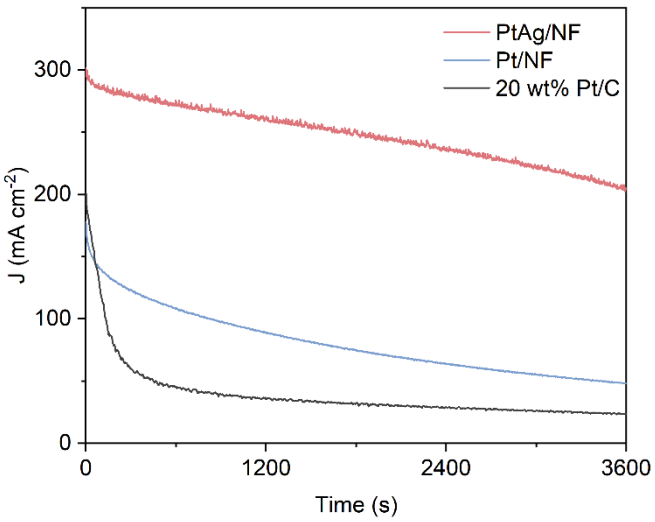

Fig. S17 Chronoamperometric measurements of Pt/NF, PtAg/NF and 20 wt% Pt/C at the applied potential of 0.7 V vs RHE in 1 M KOH with 1 M EG solution.

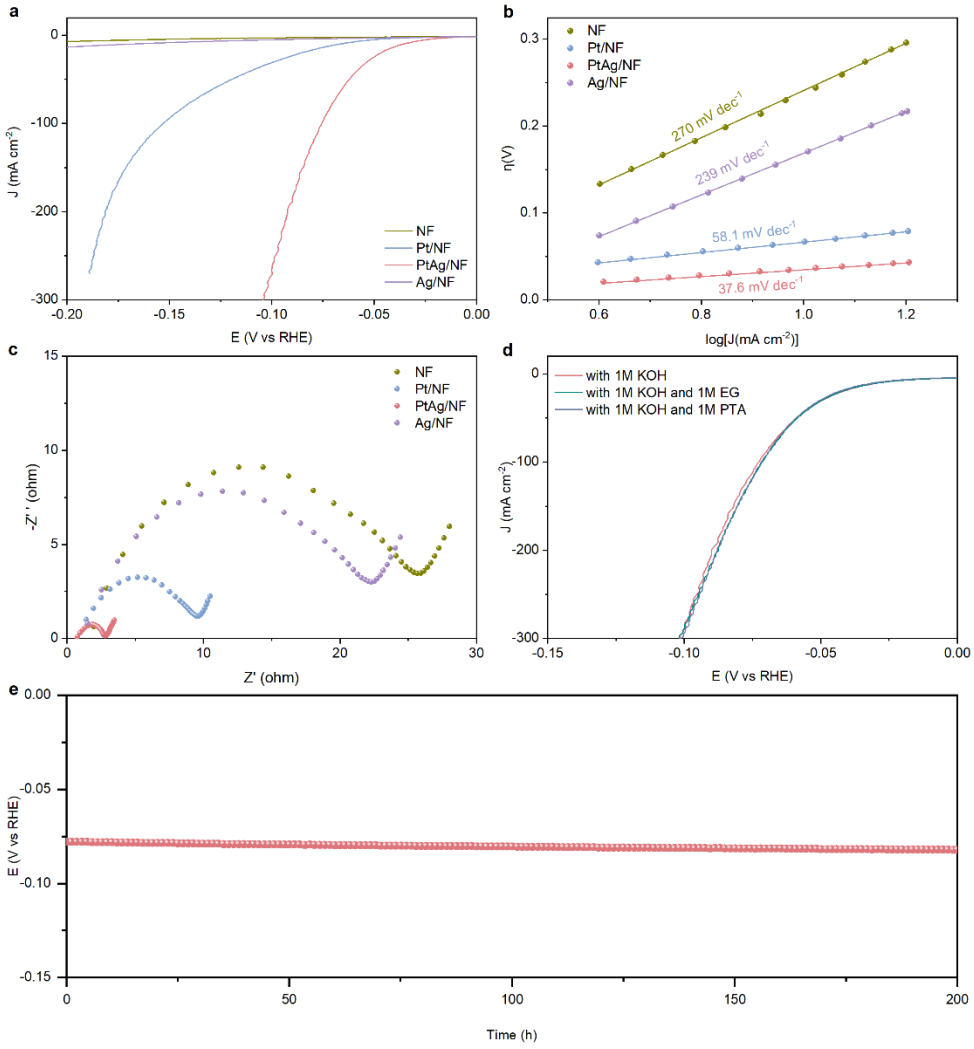

Fig. S18 a) LSV curves, b) the corresponding Tafel plots and c) Nyquist plots of NF, Pt/NF, PtAg/NF and Ag/NF for HER in 1 M KOH. d) LSV curves of PtAg/NF for HER in 1 M KOH before and after adding 1 M EG or PTA. e) The stability test of PtAg/NF for HER at 100 mA cm^{-2}.

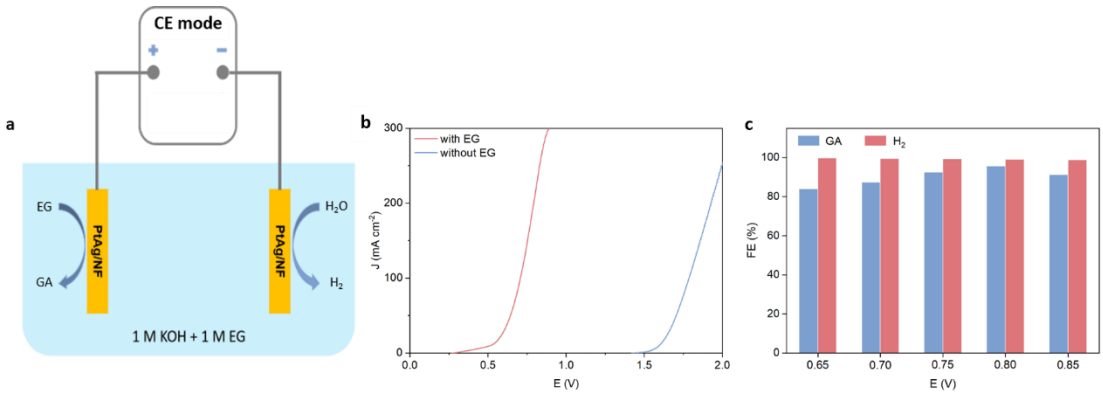

Fig. S19 a) Traditional constant electrolysis (CE) with two-electrode configuration. B) LSV curves of PtAg/NF couple in 1 M KOH with and without EG. c) The FEs of GA and H_2 over PtAg/NF couple under various voltages.

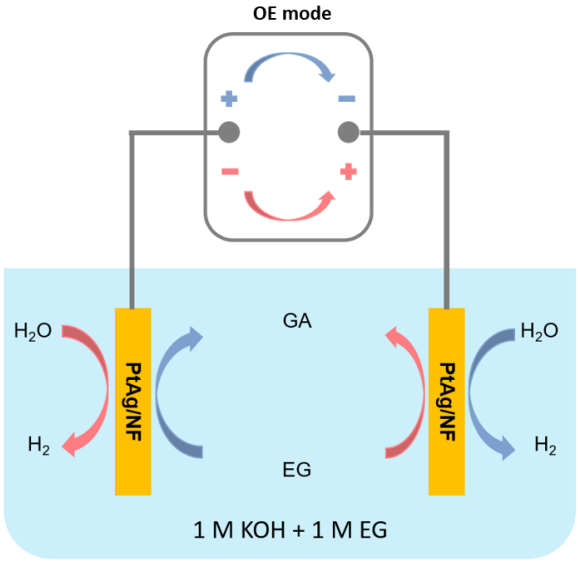

Fig. S20 Schematic of the proposed oscillation electrolysis (OE) by using PtAg/NF as both anode and cathode with two-electrode configuration for EGOR and HER.

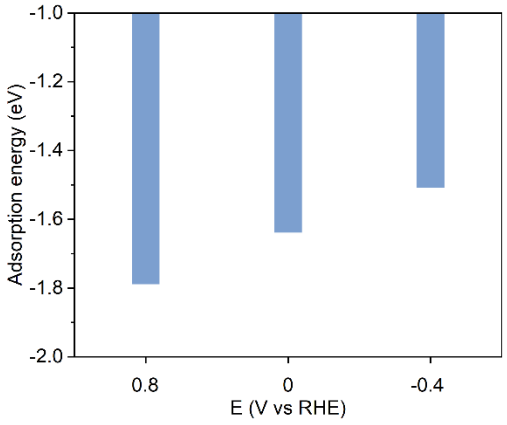

Fig. S21 The adsorption energy of CO on PtAg(111) at different potentials.

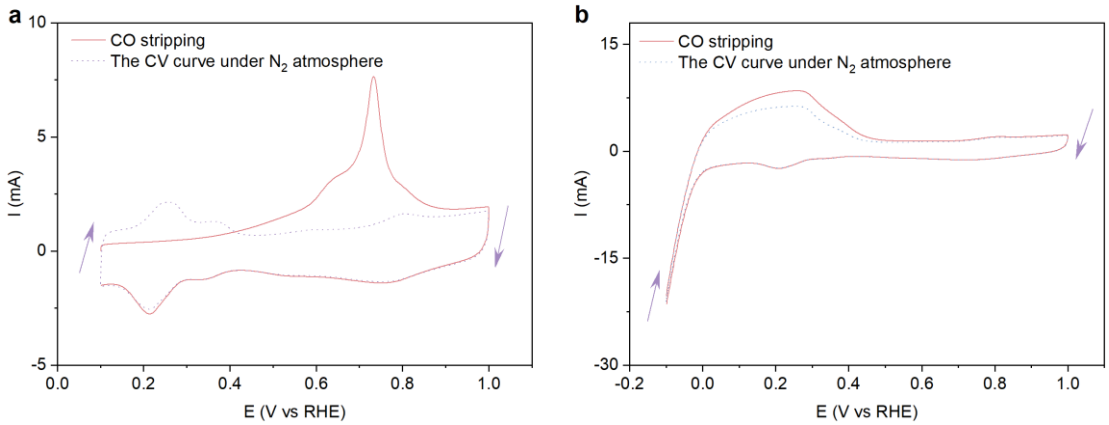

Fig. S22 CO stripping tests for PtAg under different potential windows of a) 0.1-1.0 V vs RHE (start from 0.1 V vs RHE), and b) -0.1-1.0 V vs RHE (start from -0.1 V vs RHE) in 1 M KOH at a scan rate of 50 mV s^{-1}.

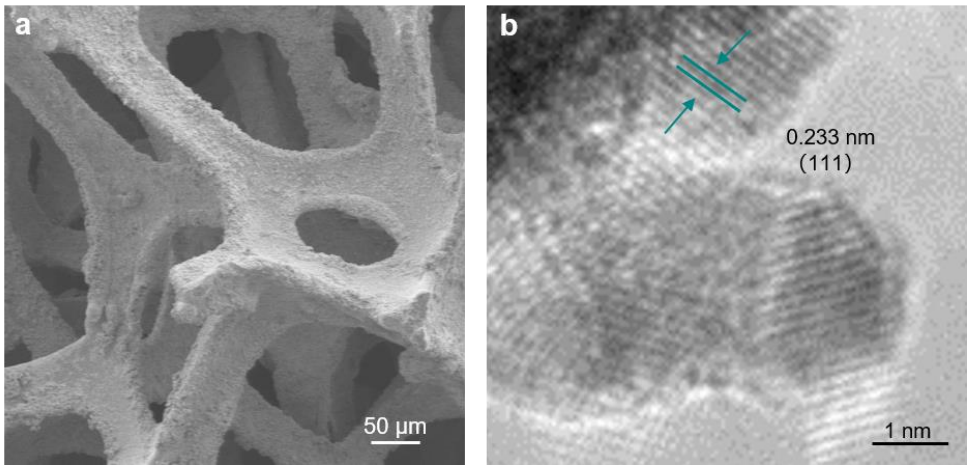

Fig. S23 a) SEM and b) HR-TEM images of PtAg/NF after stability test at 0.8 V for 100 h under the OE mode.

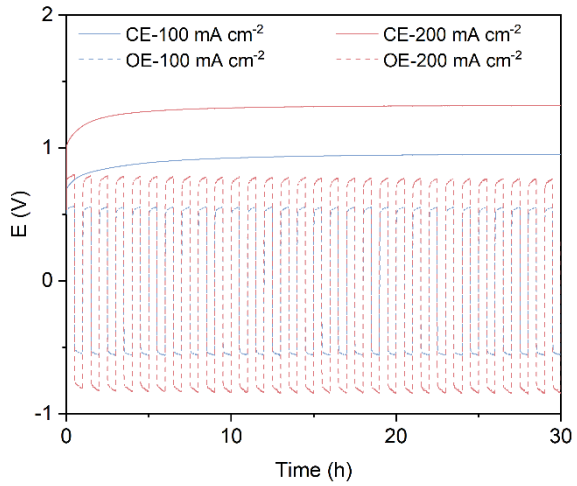

Fig. S24 Chronopotentiometric curves of PtAg/NF under OE and CE modes at 100 and 200 mA cm^{-2} in 1 M KOH with 1 M EG.

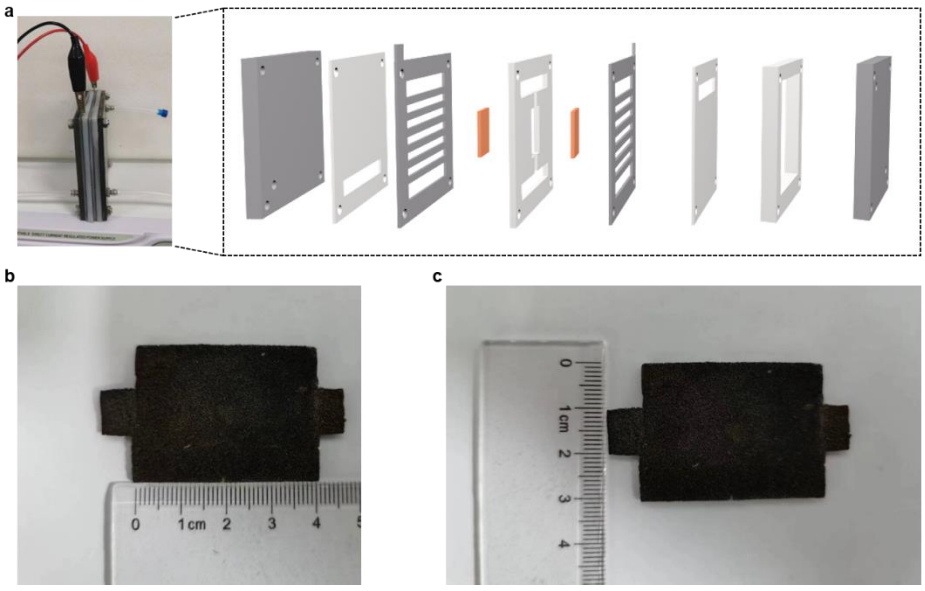

Fig. S25 a) Photograph and schematic illustration of the membrane-free flow electrolyzer, b,c) Photographs of PtAg/NF electrocatalyst.

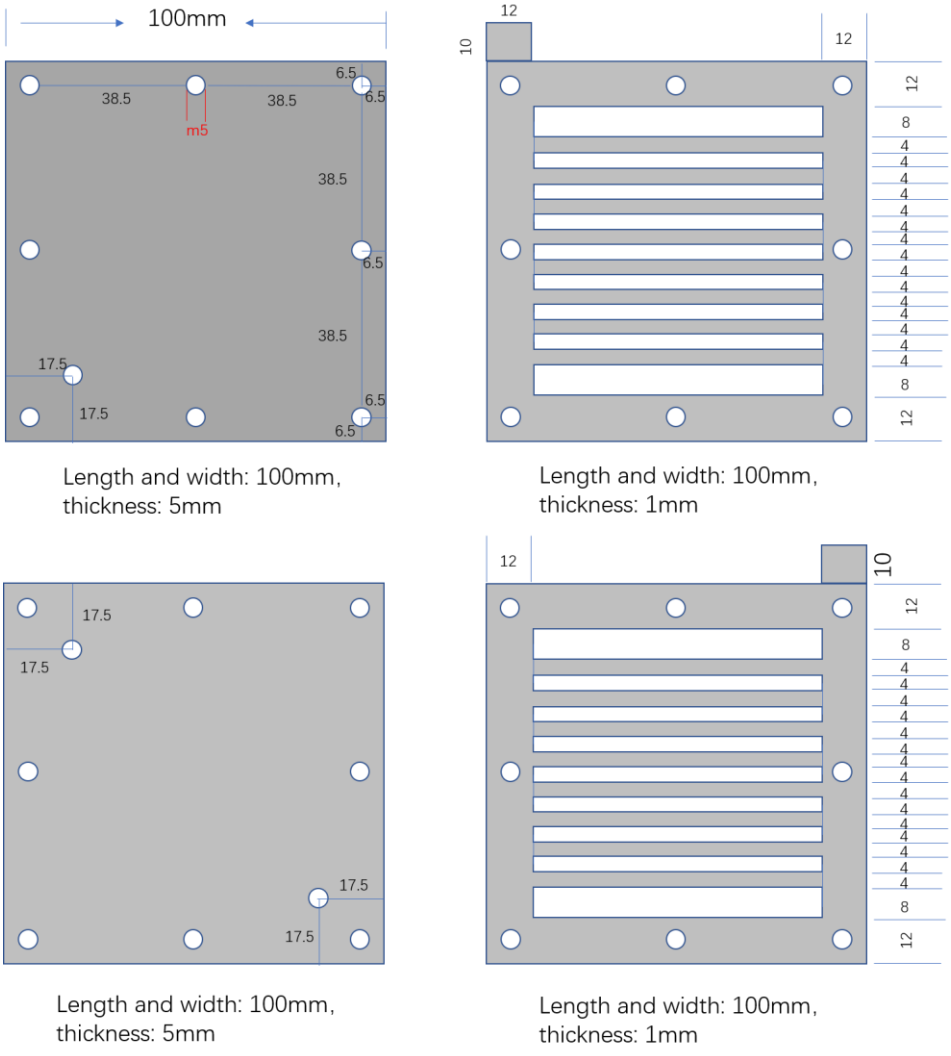

Fig. S26 Detailed dimensions of backboards and channels in flow cell.

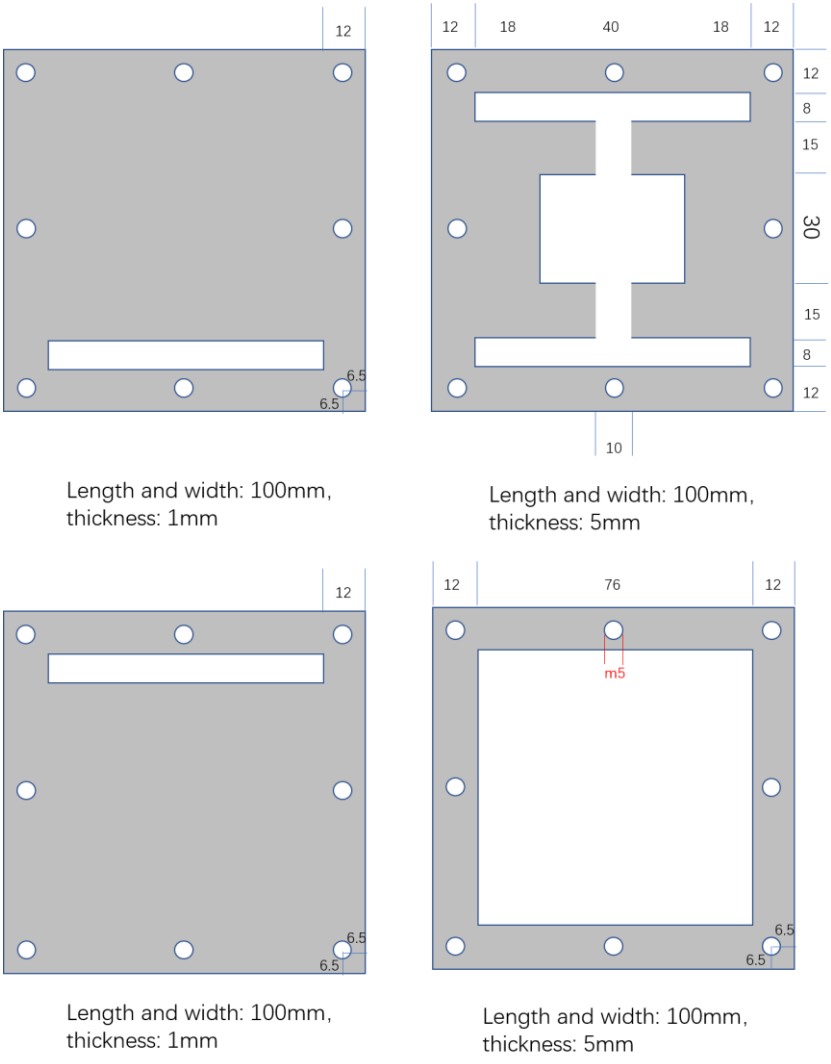

Fig. S27 Detail dimensions of silicone sheets in the flow cell.

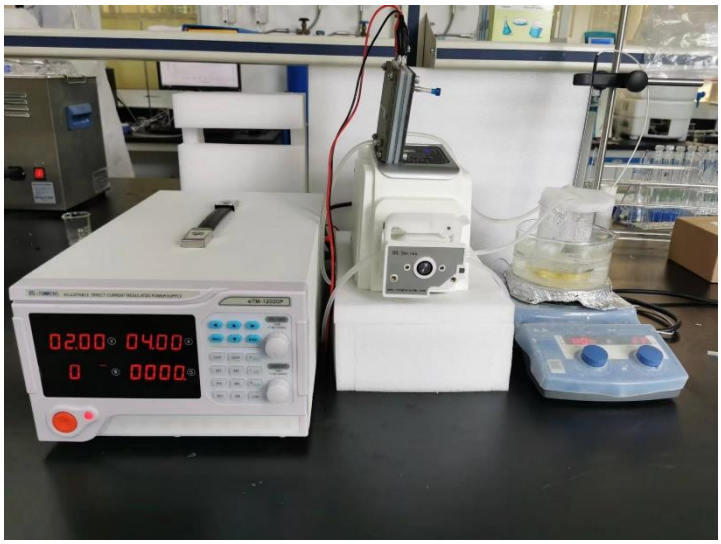

Fig. S28 Photograph of the two-electrode flow electrolyzer system. *The total volume of solution used in this process is 100 mL. The electrolyte was NOT heated, only the stirring mode of the electromagnetic stirrer was used to accelerate the diffusion of electrolyte.*

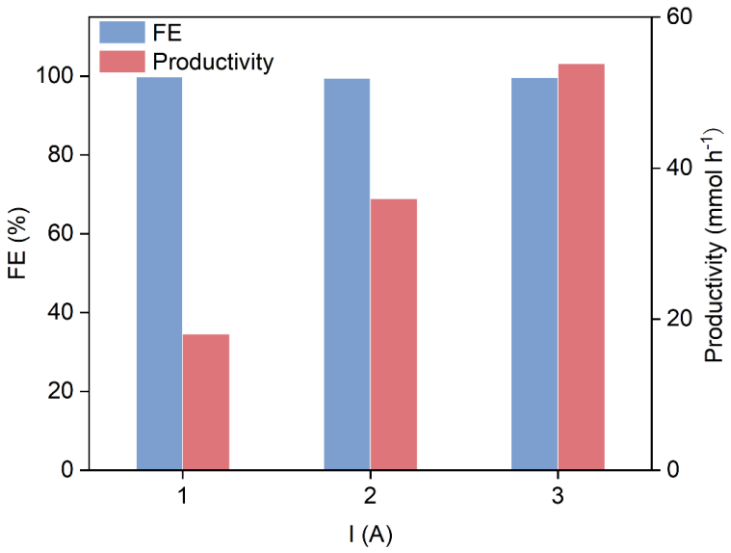

Fig. S29 FE and productivity of H_2 for PtAg/NF under different currents.

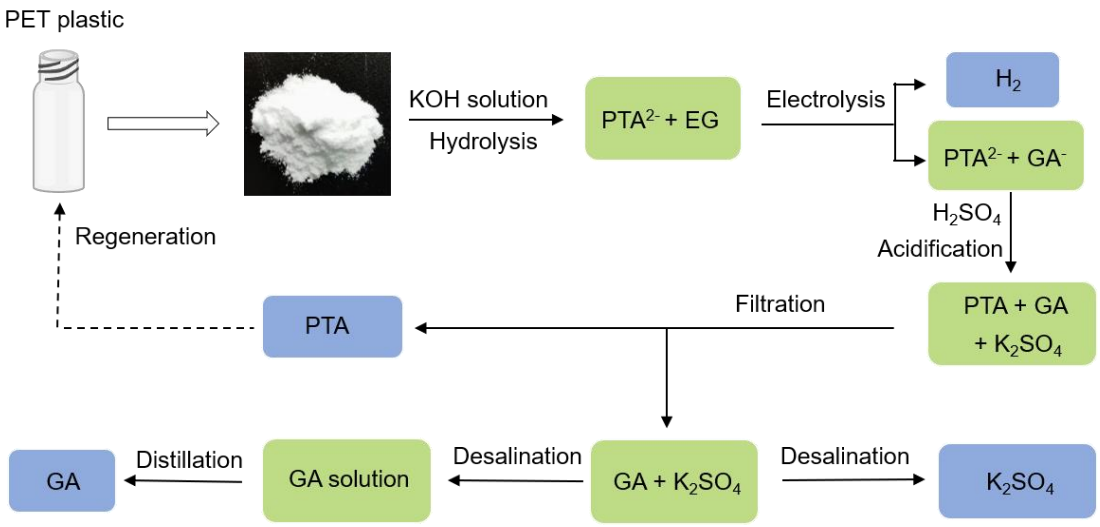

Fig. S30 Schematic of the process of PET electroreforming and product separation.

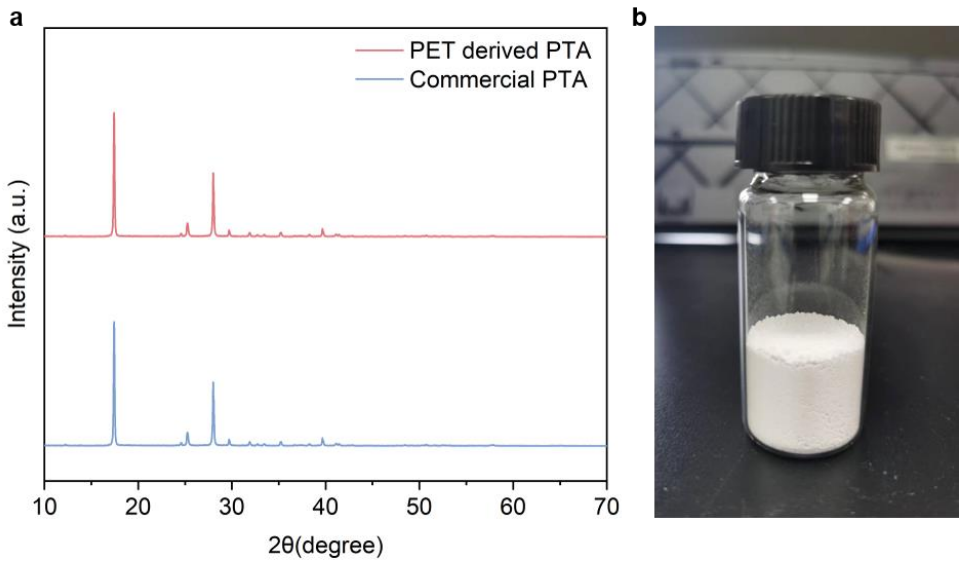

Fig. S31 a) XRD patterns of commercial PTA and PET derived PTA. b) Photograph of PET-derived PTA.

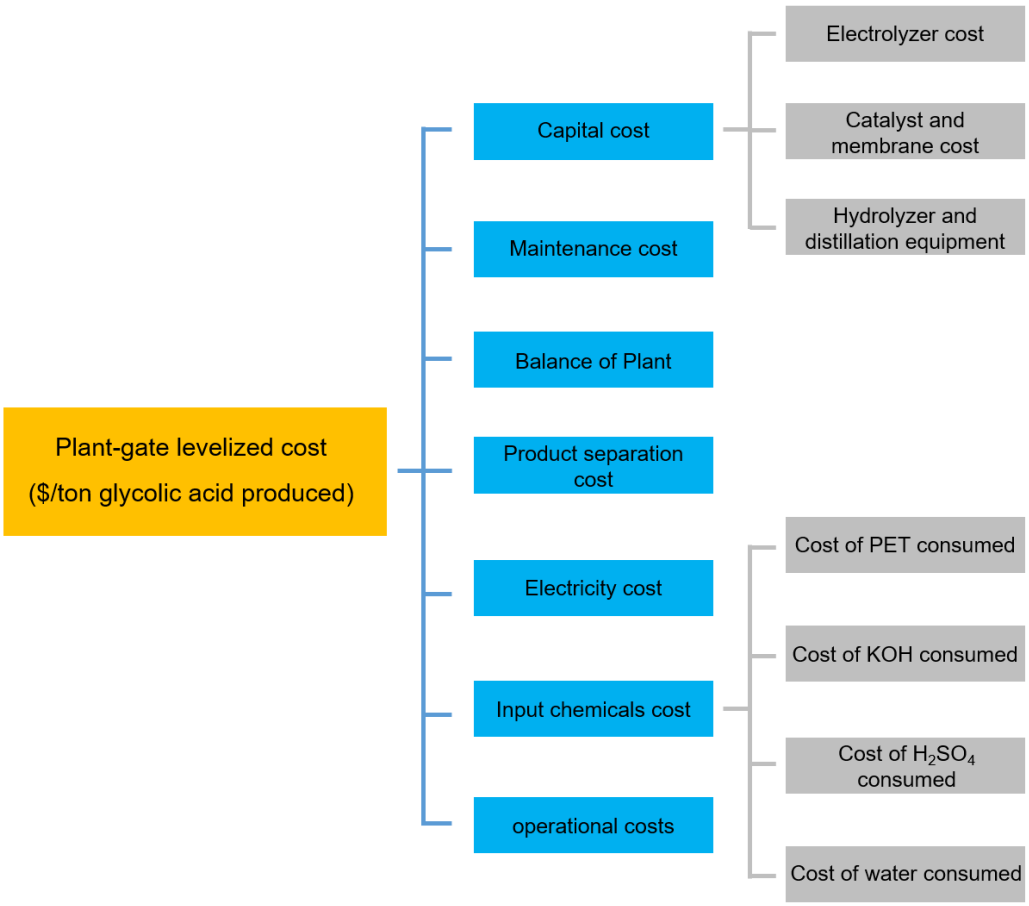

Fig. S32 Model used for the techno-economic analysis of glycolic acid production from PET via electricity. Units are US$ per ton of glycolic acid.

Supporting Note 1

To investigate the economic feasibility of our proposed oscillation electroreforming of PET and water, we carried out a simplified techno-economic analysis using a model adapted from that of literatures reported by Sargent group.[15-17] The processing capacity of the plant is 200 ton of PET waste per day. Fig. 5e,f summarize the model used to calculate the plant gate levelized cost of processing PET ($/ton PET) at different current density (100, 200, and 300 mA cm^{-2}). The price of input chemicals and products were listed in Table S2.

Below is the list of assumptions made for the calculations.

1. The capital costs of electrolyzer is sensitive to the operating current density, we assume a cost of $10,000 per m^2 of electrolyzer. The total catalyst and membrane cost are 5 % of the electrolyzer cost.[15]

2. The capital costs of hydrolyzer and distillation equipment are dependent on the process capacity of PET. Their combined cost is assumed to be 50% of PET feedstock cost.

3. The capacity factor is expected to be operational on any given day, is assumed to be 0.8, which means the plant will be operational 19.2 hours a day.[15]

4. Input chemicals include PET, potassium hydroxide, formic acid and water. The output products include GA, PTA, and H_2. The PET waste contains ~15% of unreacted impurities.[18]

5. The Faradaic efficiency and selectivity to GA from EG is 90%, and the faradaic efficiency to H_2 is assumed to be 100 %.

6. The price of electricity is assumed to be 10 ¢/kWh.[15] The electricity costs comprise 3 components, electrolyzer for EG and water electrolysis, hydrolyzer for PET hydrolysis, separation equipment for distillation and drying. The electricity costs for hydrolysis and products separation are assumed to be equal to electrolysis.

7. Both operation and maintenance costs are assumed to be 10% of the capital costs.

The calculation processes

1. Capital costs

The electrolyser cost. According to the current required and the assumed operating current density of 300 mA cm^{-2}, we can calculate the area of electrolyser needed:

$$Total\ surface\ area\ needed\ (m^2) = \frac{Total\ current\ needed\ (A)}{Current\ density\ (\frac{A}{m^2})}$$

$$Total\ current\ needed\ (A) = \frac{Plant\ capacity\ (ton/day) \times No.of\ e^-\ transfeered\ in\ reaction\ \times 96485\ (C/mol)}{Product\ molecular\ weight\ (ton/mol) \times 24(hour/day)\ \times 3600(s/hour)\ \times FE\ (\%)}$$

The electrolyser cost can be calculated based on the estimate of \$10000 per m^2. Therefore:

$$Total\ cost\ of\ electrolyzer\ (\$) = Total\ surface\ area\ needed\ (m^2)\ \times Price\ per\ m^2\ (\$/m^2)$$

The total catalyst and membrane cost are assumed to be 5 % of electrolyzer cost and is calculated as:

$$Cost\ of\ catalyst\ and\ membrane\ (\$/ton) = \frac{Total\ \text{cost of electrolyser} \times 5\%}{\text{Catalyst lifetime (year)} \times 365\ (day/year)\ \times production\ of\ product\ (ton/day)}$$

The hydrolyzer and distillation equipment are assumed to be 50% of PET and are calculated as:

$$Hydrolyzer\ and\ distillation\ equipment\ (\$/ton) = Cost\ of\ PET\ (\$/ton)\ \times 50\%$$

$$Electrolyzer\ cost\ (\$/ton) = \frac{\text{Total cost of electrolyzer (\$)}\ \times Capital\ recovery\ factor}{\text{Capacity factor}\ \times 365\ (day/year)\ \times Production\ of\ product\ (ton/day)}$$

$$Capital\ recovery\ factor = \frac{\text{Discount rate}\ \times (1 + \text{Discount rate})^{Lifetime}}{(1 + \text{Discount rate})^{Lifetime} - 1}$$

$$Capital\ costs\ (\$/ton) = Electrolyzer\ cost + catalyst\ and\ membrane\ cost + Hydrolyzer\ and\ distillation\ equipment$$

2. Maintenance cost

This is assumed to be 10% of the capital costs and is calculated as:

$$Maintenance\ cost\ (\$/ton) = \text{Capital cost}\ (\$/ton)\ \times Maintenance\ factor$$

3. Balance of plant

This is assumed to be 10% of the capital costs and is calculated as:

$$Balance\ of\ plant\ (\$/ton) = \text{Capital cost}\ (\$/ton)\ \times Balance\ of\ plant\ factor$$

4. Installation costs

This is assumed to be 10% of the capital costs and is calculated as:

$$Installation\ cost\ (\$/ton) = Capital\ cost\ (\$/ton)\ \times Lang\ factor\ (\%)$$

5. Electricity cost:

$$Electricity\ cost\ (\$/ton) = \frac{Power\ consumed\ (kW)\ \times 24\ (hour/day)\ \times Electricity\ cost\ (\$/kwh)}{Plant\ capacity\ (ton/day)}$$

$$Power\ consumed\ (kW) = \frac{Total\ current\ needed\ (A) \times Cell\ voltage\ (V)}{1000\ (W/kW)}$$

6. Input chemicals costs:

Materials require 1 ton of PET, 0.84 ton of KOH, 0.74 ton of H_2SO_4 and 20 ton of water.

$$\begin{aligned} Input\ chemicals\ (\$/ton) &= Cost\ of\ PET\ (\$/ton)\ \times Mass\ factor\ of\ PET \\ &+ Cost\ of\ KOH\ (\$/ton) \times Mass\ factor\ of\ KOH \\ &+ Cost\ of\ H_2SO_4\ (\$/ton) \times Mass\ factor\ of\ H_2SO_4 \\ &+ Cost\ of\ water\ (\$/ton) \times Mass\ factor\ of\ water \end{aligned}$$

7. Operating costs

This is assumed to be 10% of the capital costs and is calculated as:

$$Operating\ cost\ (\$/ton) = Capital\ cost\ (\$/ton) \times Operating\ factor\ (\%)$$

Finally, the total cost can be calculated by adding up all 7 components:

$$\begin{aligned} Total\ costs\ (\$/ton) &= Input\ chemicals\ (\$/ton) + Electricity\ cost\ (\$/ton) + Capital\ cost\ (\$/ton) \\ &+ Operating\ cost\ (\$/ton) + Maintenance\ cost\ (\$/ton) \\ &+ Balance\ of\ plant\ cost\ (\$/ton) + installation\ cost\ (\$/ton) \end{aligned}$$

The products of this process include terephthalic acid (PTA), glycolic acid (GA), sulfuric acid (H_2SO_4) and water (H_2O). Per ton of PET as raw material can obtain 0.72 ton PTA, 0.34 ton GA, 1.31 ton K_2SO_4 and 0.02 ton H_2.

Therefore, the product value can be calculated as:

$$\begin{aligned} Product\ value\ (\$/ton) &= Cost\ of\ PTA\ (\$/ton) \times Mass\ factor\ of\ PTA\ obtained \\ &+ Cost\ of\ GA\ (\$/ton) \times Mass\ factor\ of\ GA\ obtained \\ &+ Cost\ of\ K_2SO_4\ (\$/ton) \times Mass\ factor\ of\ K_2SO_4\ obtained \\ &+ Cost\ of\ H_2\ (\$/ton) \times Mass\ factor\ of\ H_2\ obtained \end{aligned}$$

The profit per ton of PET obtained from this process can be calculated as:

$$Profit\ (\$/ton) = Product\ value\ (\$/ton) - Total\ costs\ (\$/ton)$$

Price of feedstocks and products.

Product	Price ($/ton)	Source
Feedstocks		
Waste PET	390	a
KOH	1280	19
H_2SO_4	200	19
H_2O	0.22	19
Product		
PTA	940	18
GA	3000	b
K_2SO_4	473	19
H_2	1900	a
EG	1400	20

a: The price of PET waste was assumed to be 40% of virgin PET. (https://jiage.molbase.cn/hangqing/PET)

b: Taken from online trade market. (https://jskolod.en.made-in-china.com/product/aFlJndtVYuch/China-Potassium-Diformate-98-.html)

Table S1. The molar ratio and weight ratio of Pt/Ag in the catalyst of PtAg/NF.

Sample	The molar ratio of Pt/Ag	The weight percentage of Pt/Ag
PdAg/NF	1.45:1	72.5%/27.5%

Table S2. Comparison of EGOR to GA performance in 1.0 M KOH for PtAg/NF with other reported electrocatalysts.

Catalyst	Electrolyte	Potential (V vs RHE) (mA/cm^2)	FE (%)	Ref
PtAg/NF	1 M KOH + 1 M EG	0.7 (100)	95.7	This work
Pd-Ni(OH)$_2$/NF	1 M KOH + 1 M EG	0.69 (100)	94.1	9
Pd-N$_4$/Cu-N$_4$	1 M NaOH + 1 M EG	0.72 (10)	91.9	10
Pt/γ-NiOOH/NF	1 M KOH + 0.3 M EG	0.6 (150)	97.2	11
Au/Ni(OH)$_2$	3M KOH +0.3 M EG	1.15 (149)	91.0	12
Pd NTs/NF	1 M KOH + 0.4 M EG	0.70 (100)	87.9	13
PdAg/NF	0.5 M KOH + 1 M EG	0.57 (10)	92.0	14

Table S3. A literature survey of the stability of Pt-based EGOR electrocatalysts in alkaline electrolytes.

Catalyst	Electrolyte	Chronoamperometric stability	Ref
PtAg/NF	1 M KOH + 1M EG	84.0% (PE mode: 0.5 h)	This work
PtAg/NF	1 M KOH + 1M EG	96.4 % (OE mode: 100 h)	This work
Mo_1-PdPtNiCuZn	1 M KOH + 1 M MeOH	19.2% (14.2 h)	21
Ptc/$Ti_3C_2T_x$	1 M KOH + 1 M MeOH	42.0% (50 h)	22
PtPb@ $PtIr_1$ HNPs/C	0.5 M H_2SO_4 + 1 M EtOH	25.7% (1.0 h)	23
$PdSn_{0.5}$/Se-Ti_3C_2	1 M NaOH + 1 M MeOH	85.5% (2.8 h)	24
PdCuSn	1 M KOH + 1 M EtOH	22.6% (1.0 h)	25
PtAgNTs/C	0.5 M H_2SO_4 + 0.5 M MeOH	21.3% (0.56 h)	26
Pt_2Bi	1 M NaOH + 1 M MeOH	57.8% (2.8 h)	27
PtRu NWs	0.1 M $HClO_4$ + 0.5 M MeOH	31.3% (1.1 h)	28
PMo/Pt_4Ir_1/ MWCNT	0.5 M H_2SO_4 + 0.5 M MeOH	73.2% (0.8 h)	29
PdAgSn/PtBi HEA NPs	1 M KOH + 1 M MeOH	57.1% (2.0 h)	30
$Pd_{40}Ni_{43}P_{17}$	1 M NaOH + 1 M EtOH	5.5% (0.6 h)	31
Au@Pd nanorod	1 M NaOH + 1 M EtOH	1.7% (1.0 h)	32

Note: EG: ethylene glycol; GA: glycolate; HMF: 5-hydroxymethylfurfural; DFF: 2,5-diformylfuran; FDCA: 2,5-furandicarboxylic acid; BA: benzyl alcohol; FA: formate; EtOH: ethanol.

Table S4. Comparison of the overpotential at 10 mA cm^{-2} of HER with recently reported noble metal-based electrocatalysts in 1.0 M KOH

Catalyst	Overpotential (mV) @10 mA cm^{-2}	Tafel slope (mV dec-1)	Ref
PtAg/NF	36	38	This work
Pt-Ni(OH)x	58	89	33
Ni_2P/CoP-Pt	44	58	34
Pt/MgO	39	39	35
Pt SA-PNPM	36	33	36
Pt/MXene	34	29	37
Pt@CoS	28	31	38
Cl-Pt/LDH	24	34	39
$Pt_{SA-1.73}$-2D NiHN/NF	24	43	40
PtSA-Mn_3O_4	24	54	41
Pt_1/$(Co,Ni)(OH)_2$/C	24	28	42
PtSA/α-MoC_{1-x}@C-0.75	21	29	43
D-NiO-Pt	20	31	44
Pt_{doped}@WC_x	20	15	45
CNT-V-Fe-Ru	64	51	46
V_O-Ru/HfO_2-OP	39	29	47
RuNP-RuSA@CFN-800	33	37	48
CC@WS_2/Ru-450	32	53	49
Ru-$NiCo_2S_4$	32	41	50
Ru/P-TiO_2	27	28	51
Ru/α-MoC	25	32	52

Table S5. Recently reported catalysts for the alcohols-assisted electrochemical water splitting systems.

Catalyst	Electrolyte	Cell potential (V)(mA/cm^2)	Products	Ref
PtAg/NF	1 M KOH + 1 M EG	0.71 (100)	GA	This work
Pd-Ni(OH)$_2$/NF	1 M KOH + 1 M EG	0.93 (100)	GA	9
Pt/γ-NiOOH/NF	1 M KOH + 0.3 M EG	0.72 (100)	GA	11
Pd NTs/NF	1 M KOH + 0.4 M EG	2.48 (100)	GA	13
MoO$_x$/Pt	1 M KOH + 0.1 M G	0.70 (10)	Glycerate	53
Pt-NP/NiO-NS	1 M KOH + 1 M MeOH	1.69 (10)	FA	54
Cu(I)/Cu(II)	1.0 M KOH + 0.1 M glucose	0.92 (100)	Glucaric acid	55
NC/Ni-Mo-N/NF	1 M KOH + 0.1 M G	1.38 (10)	FA	56
MnO$_2$/CP	1 M KOH + 0.2 M G	1.38 (10)	FA	57
Ni(OH)$_2$/NF	1 M KOH + 0.5 M MeOH	1.52 (10)	FA	58
MoO$_2$-FeP@C	1.0 M KOH + 50 mM HMF	1.486 (10)	FDCA	59
Co(OH)$_2$@ HOS/ CP	1 M KOH + 3 M MeOH	1.497 (10)	FA	60
Co-S-P/CC	1 M KOH + 1 M E	1.63 (10)	Acetic acid	61

Note: EG: ethylene glycol; GA: glycolate; FA: formate; G: glycerinum; MeOH: methyl alcohol; E: ethanol; HMF: 5-hydroxymethylfurfural; FDCA: 2,5-furandicarboxylic acid.

9. Supplementary References

1 B. Deng, M. Huang, K. Li, X. Zhao, Q. Geng, S. Chen, H. Xie, X. Dong, H. Wang, F. Dong, *Angew. Chem. Int. Ed.*, 2022, **61**, e202114080.
2 Z. Chen, T. Wang, B. Liu, D. Cheng, C. Hu, G. Zhang, W. Zhu, H. Wang, Z. J. Zhao, J. Gong, *J. Am. Chem. Soc.*, 2020, **142**, 6878.
3 H. Miyake, S. Ye, M. Osawa, *Electrochem. Commun.*, 2002, **4**, 973.
4 G. Kresse, J. Furthmüller, *Comput. Mater. Sci.*, 1996, **6**, 15-50.
5 G. Kresse, J. Furthmüller, *Phys. Rev. B*, 1996, **54**, 11169-11186.
6 G. Kresse, J. Hafner, *Phys. Rev. B*, 1993, **48**, 13115-13118.
7 J. P. Perdew, J. A. Chevary, S. H. Vosko, K. A. Jackson, M. R. Pederson, D. J. Singh, C. Fiolhais, *Phys. Rev. B*, 1992, **46**, 6671-6687.
8 H. J. Monkhorst, J. D. Pack, *Phys. Rev. B*, 1976, **13**, 5188-5192.
9 F. Liu, X. Gao, R. Shi, Z. Guo, E. C. M. Tse, Y. Chen, *Angew. Chem. Int. Ed.*, 2023, **62**, e202300094.
10 E. A. Moges, C.-Y. Chang, W.-H. Huang, K. Lakshmanan, Y. A. Awoke, C.-W. Pao, M.-C. Tsai, W.-N. Su, B. H. Hwang, *Adv. Funct. Mater.*, 2022, **32**, 2206887.
11 M. Du, Y. Zhang, S. Kang, C. Xu, Y. Ma, L. Cai, Y. Zhu, Y. Chai, B. Qiu, *Small*, 2023, **19**, 2303693.
12 Y. Y, H. Zhou, S.-M. Xu, J. Yang, P. Hao, X. Cai, Y. Ren, M. Xu, X. Kong, M. S., Z. Li, H. Duan, *J. Am. Chem. Soc.*, 2023, **145**, 6144-6155.
13 T. Ren, Z. Duan, H. Wang, H. Yu, K. Deng, Z. Wang, H. Wang, L. Wang, Y. Xu, *ACS Catal.*, 2023, **13**, 10394-10404.
14 D. Si, B. Xiong, L. Chen, J. Shi, *Chem Catal.*, 2021, **1**, 941-955.
15 W. Leow, Y. Lum, A. Ozden, Y. Wang, D.-H. Nam, B. Chen, J. Wicks, T.-T. Zhuang, F. Li, D. Sinton, E. H. Sargent, *Science*, 2020, **368**, 1228-1233.
16 Y. Lum, J. E. Huang, Z. Wang, M. Luo, D.-H. Nam, W. R. Leow, B. Chen, J. Wicks, Y. C. Li, Y. Wang, C.-T. Dinh, J. Li, T.-T. Zhuang, F. Li, T.-K. Sham, D. Sinton, E. H. Sargent, *Nat. Catal.*, 2020, **3**, 14-22.
17 P. D. Luna, C. Hahn, D. Higgins, S. A. Jaffer, T. F. Jaramillo, E. H. Sargent, *Science*, 2020, **367**, 6482.
18 T. Uekert, C. M. Pichler, T. Schubert, E. Reisner, *Nat. Sustain.*, 2021, **4**, 383-391.
19 W.-J. Liu, Z. Xu, D. Zhao, X.-Q. Pan, H.-C. Li, X. Hu, Z.-Y. Fan, W.-K. Wang, G.-H. Zhao, S. Jin, G. W. Hube, H.-Q. Yu, *Nat. Commun.*, 2020, **11**, 265.
20 O. S. Bushuyev, P. D. Luna, C. T. Dinh, L. Tao, G. Saur, J. Lagemaat, S. O. Kelley, E. H. Sargent, *Joule*, 2018, **2**, 825-832.
21 L. He, M. Li, L. Qiu, S. Geng, Y. Liu, F. Tian, M. Luo, H. Liu, Y. Yu, W. Yang, S. Guo, *Nat. Commun.*, 2024, **15**, 2290.
22 J. Zhu, L. Xia, R. Yu, R. Lu, J. Li, R. He, Y. Wu, W. Zhang, X. Hong, W. Chen, Y. Zhao, L. Zhou, L. Mai, Z. Wang, *J. Am. Chem. Soc.*, 2022, **144**, 15529-15538.
23 G. Zhang, D. Cao, S. Guo, Y. Fang, Q. Wang, S. Cheng, W. Zuo, Z. Yang, P. Cui, *Small*, 2022, **18**, 2202587.
24 S. Chen, N. Liu, J. Zhong, R. Yang, B. Yan, L. Gan, P. Yu, X. Gui, H. Yang, D. Yu, Z. Zeng, G. Yang, *Angew. Chem. Int. Ed.*, 2022, **61**, e202209693.
25 M. Zhou, J. Liu, C. Ling, Y. Ge, B. Chen, C. Tan, Z. Fan, J. Huang, J. Chen, Z. Liu, Z. Huang, J. Ge, H. Cheng, Y. Chen, L. Dai, P. Yin, X. Zhang, Q. Yun, H. Zhang, *Adv. Mater.*, 2022, **34**, 2106115.
26 Y. Ouyang, H. Cao, H. Wu, D. Wu, F. Wang, X. Fan, W. Yuan, M. He, L. Zhang, C. Li, *Appl. Catal. B: Environ*., 2020, **265**, 118606.
27 X. Yuan, X. Jiang, M. Cao, L. Chen, K. Nie, Y. Zhang, Y. Xu, X. Sun, Y. Li, Q. Zhang, *Nano Res*., 2019, **12**, 429-436.
28 L. Huang, X. Zhang, Q. Wang, Y. Han, Y. Fang, S. Dong, *J. Am. Chem. Soc*., 2018, **140**, 1142-1147.
29 J. Yuan, B. He, L. Hong, J. Lu, J. Miao, L. Niu, *J. Mater. Chem*., 2012, **22**, 19658-19665.
30 X. Lao, X. Liao, C. Chen, J. Wang, L. Yang, Z. Li, J.-W. Ma, A. Fu, H. Gao, P. Guo, *Angew. Chem. Int. Ed*., 2023, **135**, e202304510.
31 L. Chen, L. Lu, H. Zhu, Y. Chen, Y. Huang, Y. Li, L. Wang, *Nat. Commun.*, 2017, **8**, 14136.

32 X. Zhou, Y. Ma, Y. Ge, S. Zhu, Y. Cui, B. Chen, L. Liao, Q. Yun, Z. He, H. Long, L. Li, B. Huang, Q. Luo, L. Zhai, X. Wang, L. Bai, G. Wang, Z. Guan, Y. Chen, C.-S. Lee, J. Wang, C. Ling, M. Shao, Z. Fan, H. Zhang, *J. Am. Chem. Soc.*, 2022, **144**, 547-555.
33 Q. Li, Q. Zhang, W. Xu, R. Zhao, M. Jiang, Y. Gao, W. Zhong, K. Chen, Y. Chen, X. Li, N. Yang, *Adv. Energy Mater.*, 2023, **13**, 2203955.
34 Y. Tan, J. Feng, H. Dong, L. Liu, S. Zhao, F. Lai, T. Liu, Y. Bai, I. P. Parkin, G. He, *Adv. Funct. Mater.*, 2023, **33**, 2209967.
35 H. Tan, B. Tang, Y. Lu, Q. Ji, L. Lv, H. Duan, N. Li, Y. Wang, S. Feng, Z. Li, C. Wang, F. Hu, Z. Sun, W. Yan, *Nat. Commun.*, 2022, **13**, 2024.
36 W. Peng, J. Han, Y.-R. Lu, M. Luo, T.-S. Chan, M. Peng, Y. Tan, *ACS Nano*, 2022, **16**, 4116.
37 Y. Wu, W. Wei, R. Yu, L. Xia, X. Hong, J. Zhu, J. Li, L. Lv, W. Chen, Y. Zhao, L. Zhou, L. Mai, *Adv. Funct. Mater.*, 2022, **32**, 2110910.
38 A. Mosallanezhad, C. Wei, P. Ahmadian Koudakan, Y. Fang, S. Niu, Z. Bian, B. Liu, T. Huang, H. Pan, G. Wang, *Appl. Catal. B: Environ.*, 2022, **315**, 121534.
39 T. Zhang, J. Jin, J. Chen, Y. Fang, X. Han, J. Chen, Y. Li, Y. Wang, J. Liu, L. Wang, *Nat. Commun.*, 2022, **13**, 6875.
40 H. T. Le, D. T. Tran, T. H. Nguyen, V. A. Dinh, N. H. Kim, J. H. Lee, *Appl. Catal. B: Environ.*, 2022, **317**, 121684.
41 J. Wei, K. Xiao, Y. Chen, X.-P. Guo, B. Huang, Z.-Q. Liu, *Energy Environ. Sci.*, 2022, **15**, 4592-4600.
42 A. Pei, R. Xie, Y. Zhang, Y. Feng, W. Wang, S. Zhang, Z. Huang, L. Zhu, G. Chai, Z. Yang, Q. Gao, H. Ye, C. Shang, B. H. Chen, Z. Guo, *Energy Environ. Sci.*, 2023, **16**, 1035.
43 W. Wang, Y. Wu, Y. Lin, J. Yao, X. Wu, C. Wu, X. Zuo, Q. Yang, B. Ge, L. Yang, G. Li, S. Chou, W. Li, Y. Jiang, *Adv. Funct. Mater.*, 2022, **32**, 2108464.
44 Y. Yan, J. Lin, T. Xu, B. Liu, K. Huang, L. Qiao, S. Liu, J. Cao, S. C. Jun, Y. Yamauchi, J. Qi, *Adv. Energy Mater.*, 2022, **12**, 2200434.
45 T. Ma, H. Cao, S. Li, S. Cao, Z. Zhao, Z. Wu, R. Yan, C. Yang, Y. Wang, P. A. van Aken, L. Qiu, Y. Wang, C. Cheng, *Adv. Mater.*, 2022, **34**, 2206368.
46 T. Gao, X. Tang, X. Li, S. Wu, S. Yu, P. Li, D. Xiao, Z. Jin, *ACS Catal.*, 2023, **13**, 49-59.
47 G. Li, H. Jang, S. Liu, Z. Li, M. G. Kim, Q. Qin, X. Liu, J. Cho, *Nat. Commun.*, 2022, **13**, 1270.
48 T. Luo, J. Huang, Y. Hu, C. Yuan, J. Chen, L. Cao, K. Kajiyoshi, Y. Liu, Y. Zhao, Z. Li, Y. Feng, *Adv. Funct. Mater.*, 2023, **33**, 2213058.
49 J. Li, Y. Li, J. Wang, C. Zhang, H. Ma, C. Zhu, D. Fan, Z. Guo, M. Xu, Y. Wang, H. Ma, *Adv. Funct. Mater.*, 2022, **32**, 2109439.
50 H. Su, S. Song, Y. Gao, N. Li, Y. Fu, L. Ge, W. Song, J. Liu, T. Ma, *Adv. Funct. Mater.*, 2022, **32**, 2109731.
51 S. Zhou, H. Jang, Q. Qin, L. Hou, M. G. Kim, S. Liu, X. Liu, J. Cho, *Angew. Chem. Int. Ed.*, 2022, **61**, e202212196.
52 X. Fan, C. Liu, M. Wu, B. Gao, L. Zheng, Y. Zhang, H. Zhang, Q. Gao, X. Cao, Y. Tang, *Appl. Catal. B: Environ.*, 2022, **318**, 121867.
53 X. Yu, E. C. dos Santos, J. White, G. Salazar-Alvarez, L. G. M. Pettersson, A. Cornell, M. Johnsson, *Small* 2021, **17**, 2104288.
54 G. Ma, X. Zhang, G. Zhou, X. Wang, *Chem. Eng. J.* 2021, **411**, 128292.
55 Y. Zhang, B. Zhou, Z. Wei, W. Zhou, D. Wang, J. Tian, T. Wang, S. Zhao, J. Liu, L. Tao, S. Wang, *Adv. Mater.* 2021, **33,** e2104791.
56 Y. Xu, M. Liu, S. Wang, K. Ren, M. Wang, Z. Wang, X. Li, L. Wang, H. Wang, *Appl. Catal., B* 2021, **298,** 120493.
57 Y. Li, X. Wei, S. Han, L. Chen, J. Shi, *Angew. Chem. Int. Ed.* 2021, **60,** 21464-21472.
58 J. Hao, J. Liu, D. Wu, M. Chen, Y. Liang, Q. Wang, L. Wang, X.-Z. Fu, J.-L. Luo, *Appl. Catal., B* 2021, **281,** 119510.
59 G. Yang, Y. Jiao, H. Yan, Y. Xie, A. Wu, X. Dong, D. Guo, C. Tian, H. Fu, *Adv. Mater.* 2020, **32,** e2000455.
60 K. Xiang, D. Wu, X. Deng, M. Li, S. Chen, P. Hao, X. Guo, J.-L. Luo, X.-Z. Fu, *Adv. Funct. Mater.* 2020, **30,** 1909610.
61 S. Sheng, K. Ye, L. Sha, K. Zhu, Y. Gao, J. Yan, G. Wang, D. Cao, *Inorg. Chem. Front.* 2020, **7,** 44984506.